Pergamon

Int. J. Heat Mass Transfer. Vol. 40, No. 9, pp. 2081–2096, 1997

0017–9310/97 $17.00 + 0.00

PII: S0017–9310(96)00289–X

A recursive least-squares algorithm for on-line 1-D inverse heat conduction estimation

CHING-CHINA JI, PAN-CHIO TUAN and HORNG-YUNG JANG

Department of System Engineering, Chung-Cheng Institute of Technology, Ta-Chi, Tao-Yuan, Taiwan 33509, Republic of China

(*Received* 19 *October* 1995 *and in final form* 19 *July* 1996)

Abstract—The recursive least-squares algorithm was adopted to investigate the estimation of surface heat flux of inverse heat conduction problem from experimental data. The Kalman filtering technique which accounted for the residual innovation sequence and the least-squares estimation which accounted for computing heat flux was introduced to treat one-dimensional inverse heat conduction problem. By virtue of recursive algorithm, an on-line estimation can be made in place of batch form off-line estimation. The method is adequate for impulse heat flux estimation. © 1997 Elsevier Science Ltd. All rights reserved.

1. INTRODUCTION

The inverse heat conduction problem (IHCP), opposite to direct heat conduction problem (DHCP), deals with determining unknown conditions, material properties, and energy generation with the measurement of surface temperature. The analytical and numerical techniques proposed for solving such problems include, among many others, the analytic solution developed by using integral or Laplace transform technique [1–5], the numerical methods which include the sequential estimation technique [6–9], the least-squares method modified by the addition of regularization term [6], and the conjugate gradient method with adjoint equation [10–14]. They are almost belonging to so called batch or global form estimation methods because they utilize all measurement records to estimate the unknown components.

In some situations, it is necessary to estimate the history of unknown properties in real time, for example, to monitor the status of nuclear reaction by inverse method in order to avoid any accident. Because of the importance of real time estimation in engineering applications, the recursive input estimation algorithm of digital estimation theory is proposed [15–18]; it is based on the concept of Kalman filtering technique and the least-squares estimation of recursive processing. The Kalman filter is used to generate the residual innovation sequence and the least-squares algorithm is used for computing the magnitude of heat flux. The philosophy of this algorithm is similar to the IHCP, in which the state of system modeling is temperature and the input parameter to be estimated is heat flux. Tuan *et al.* [19] successfully solves the two-dimensional inverse heat conduction problem by using a recursive input estimator to estimate a time varying sudden change heat flux.

In this study, an experimental apparatus is facilitated to measure temperature. With these experimental data, an inverse analysis utilizing the recursive input estimation algorithm is used to estimate the unknown heat flux simultaneously. By means of the estimated heat flux, the DHCP is used to solve the temperature profile with time in copper plate. A comparison is made with the measured temperature and the estimated temperature at a point in order to investigate real time recursive estimation algorithm.

2. THEORY

The IHCP involves the estimation of boundary conditions and thermal properties provided that certain transient temperature measurements are known. In this paper, our objective is, by utilizing the measured temperature data, to estimate the unknown surface heat flux $G(t)$, with recursive input estimation algorithm. Therefore, the first step is to transform the governing equation into the state equation. Because of the need of estimation in real time, the second step is to use the recursive least-squares algorithm (RLSA) method to get the estimation of acting heat flux.

In this paper, a one-dimensional heat conduction model through copper plate is assumed with thermal insulated at $x = x_s$ and all surfaces except at $x = 0$ surface, a uniform heat flux $G(t)$ is acting. The geometry and coordinates is shown in Fig. 1. The dimensional energy equation is written as

$$\frac{\partial T}{\partial t} = \alpha \frac{\partial^2 T}{\partial x^2} \quad 0 \leqslant x \leqslant x_s, \quad t > 0 \tag{1}$$

the associated boundary conditions are taken as

$$-\kappa \frac{\partial T(0,t)}{\partial x} = G(t) = ?(\text{to be estimated}) \quad t > 0 \tag{2}$$

NOMENCLATURE

$\mathbf{H}$	measurement matrix defined by equation (9)
K	Kalman gain
N	the numbers of data points
P	filter's error covariance matrix
P_b	error covariance matrix
Q	process noise covariance
$G(t)$	heat flux to be estimated [cal cm^{-2} s^{-1}]
R	measurement noise covariance ($=\sigma^2$)
$T(x,t)$	computed temperature [°C]
T_0	initial temperature [°C]
Δt	sampling interval [s]
x	dimensional axial coordinate [cm]
$\mathbf{X}$	state vector defined by equation (8)
$Y(t)$	the measured temperature corrupted by noise [°C]
$\mathbf{Z}$	observation vector defined by equation (9).

Greek alphabet

α	thermal diffusivity [cm^2 s^{-1}]
γ	fading factor
Γ	input matrix defined by equation (8)
δ	Dirac-delta function
κ	thermal conductivity [cal cm^{-1}°C^{-1} s^{-1}]
$v(t)$	the measured noise assumed zero mean and white Gaussian noise
σ	standard deviation
$\mathbf{\Phi}$	the state transition matrix defined by equation (8)
$\mathbf{\Psi}$	coefficient matrix defined by equation (7)
$\mathbf{\Omega}$	coefficient matrix defined by equation (7).

Superscripts

$\hat{}$	estimated
$-$	estimated by filter
T	transpose of matrix.

Subscripts

k	the discretized time step.

$$\frac{\partial T(x_s,t)}{\partial x}=0 \quad t>0 \tag{3}$$

and the initial condition as

$$T(x,0)=T_0 \quad 0\leqslant x\leqslant x_s \tag{4}$$

with measurements

$$Y(t)=T(x_s,t)+v(t) \quad t>0 \tag{5}$$

here α is the thermal diffusivity, κ is the thermal conductivity, T_0 is the initial temperature, $G(t)$ is the heat flux to be estimated, $Y(t)$ is the measured temperature corrupted by noise, and $v(t)$ is the measurement noise assumed zero mean and white Gaussian noise. Before we transform the governing equations (1–4) to discrete-time state equations, the continuous-time state equation is derived first. The central difference approximation for the spaces derivative is used.

$$\dot{T}_i(t)=\alpha\frac{T_{i+1}(t)-2T_i(t)+T_{i-1}(t)}{\Delta x^2} \qquad i=0,1,2,\ldots,n-1. \tag{6}$$

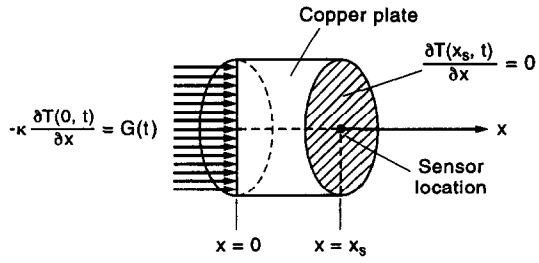

Fig. 1. Geometry and coordinates.

In cooperation with boundary conditions, equations (2)–(3), we get the continuous-time state equation as follows

$$\dot{\mathbf{T}}(t)=\mathbf{\Psi}\mathbf{T}(t)+\mathbf{\Omega}G(t) \tag{7}$$

where

$$\mathbf{T}(t)=[T_0(t) \quad T_1(t) \quad \ldots, \quad T_{n-1}(t)]^{\mathrm{T}}$$

$$\mathbf{\Psi}=\frac{\alpha}{\Delta x^2}\begin{bmatrix} -2 & 2 & & & \mathbf{O} \\ 1 & 2 & 1 & & \\ & \cdots & \cdots & & \\ & & \cdots & \cdots & \\ & & 1 & 2 & 1 \\ \mathbf{O} & & & 2 & -2 \end{bmatrix}$$

$$\mathbf{\Omega}=\left[\frac{2\alpha}{\kappa\Delta x}0 \quad 0 \quad 0 \quad \ldots \quad 0\right]^{\mathrm{T}}$$

and the system process model is

$$\mathbf{X}_{k+1}=\mathbf{\Phi}\mathbf{X}_k+\mathbf{\Gamma}G_k \tag{8}$$

where

$$\mathbf{X}_k=[T_{0,k} \quad T_{1,k} \quad \ldots, \quad T_{n-1,k}]^{\mathrm{T}}$$

$$\mathbf{\Phi}=e^{\mathbf{\Psi}\Delta t}$$

$$\mathbf{\Gamma}=\int_{k\Delta t}^{(k+1)\Delta t} e^{[\mathbf{\Psi}(k+1)\Delta t-\tau]}\mathbf{\Omega}\,d\tau$$

here $\mathbf{X}_k$ is the state vector, $\mathbf{\Phi}$ is the state transition matrix, $\mathbf{\Gamma}$ is input matrix, G_k is the sequence of deterministic input and k is the discretized time step index. The measurement equation is

$$\mathbf{Z}_{k+1} = \mathbf{H}\mathbf{X}_{k+1} + v_{k+1} \tag{9}$$

where

$$\mathbf{H} = [0 \quad 0 \quad 0 \quad , \ldots , \quad 1].$$

here v_{k+1} is the measurement noise, random sequences with zero mean. $\mathbf{H}$ is the measurement matrix, $\mathbf{Z}_k$ is the observation vector at time k, and v_k is the measurement noise vector which is assumed to be zeros mean white noise with variance $E\{v_k v_j^{\mathrm{T}}\} = R\delta_{kj}$, R is the measurement noise covariance and δ is the Dirac delta function. Following the general notation of the Kalman filter equations [20], when a heat flux occurs, the posterior estimation of $\mathbf{X}_k$ is

$$\hat{\mathbf{X}}_{k/k} = (\mathbf{I} - \mathbf{K}_k\mathbf{H})\hat{\mathbf{X}}_{k/k-1} + \mathbf{K}_k\mathbf{Z}_k \tag{10}$$

$$\hat{\mathbf{X}}_{k/k-1} = \mathbf{\Phi}\hat{\mathbf{X}}_{k-1/k-1} + \mathbf{\Gamma}G_{k-1} \tag{11}$$

$$\mathbf{K}_k = \mathbf{P}_{k/k-1}\mathbf{H}^{\mathrm{T}} + (\mathbf{H}\mathbf{P}_{k/k-1}\mathbf{H}^{\mathrm{T}} + \sigma_k^2)^{-1} \tag{12}$$

$$\mathbf{P}_{k/k-1} = \mathbf{\Phi}\mathbf{P}_{k-1/k-1}\mathbf{\Phi}^{\mathrm{T}} + \mathbf{\Gamma}\mathbf{Q}\mathbf{\Gamma}^{\mathrm{T}} \tag{13}$$

$$\mathbf{P}_{k/k} = (\mathbf{I} - \mathbf{K}_k\mathbf{H})\mathbf{P}_{k/k-1}. \tag{14}$$

Let $\hat{\mathbf{X}}_{k/k}$ and $\bar{\mathbf{X}}_{k/k}$ differently denote the estimation of the true state $\mathbf{X}_k$ with or without G_{k-1}. From equations (10)–(11), we get

$$\hat{\mathbf{X}}_{k/k} = (\mathbf{I} - \mathbf{K}_k\mathbf{H})(\mathbf{\Phi}_{k-1}\hat{\mathbf{X}}_{k-1/k-1} + \mathbf{\Gamma}G_{k-1}) + \mathbf{K}_k\mathbf{Z}_k \tag{15}$$

and

$$\bar{\mathbf{X}}_{k/k} = (\mathbf{I} - \mathbf{K}_k\mathbf{H})\mathbf{\Phi}_{k-1}\hat{\mathbf{X}}_{k-1/k-1} + \mathbf{K}_k\mathbf{Z}_k. \tag{16}$$

For simplicity, consider $G_k = G$ in equation (8) to be a constant over the certain interval, for $k = n, n+1, \ldots, n+l$, as below

$$G_k = \begin{cases} 0, & k \leqslant n \\ G, & n < k \leqslant n+l \end{cases} \tag{17}$$

where n represents heat flux starting time which is unknown. This assumption is reasonable if $l\Delta T$ is small compared with the presence of entire period of the heat flux $\lambda\Delta T$, i.e. $l\Delta T < \lambda\Delta T$. Let $\Delta\mathbf{X}_k = \hat{\mathbf{X}}_{k/k} - \bar{\mathbf{X}}_{k/k}$ and $G_{k-1} = 0$ for $k \leqslant n$. Subtracting equation (16) from equation (15), yields

$$\Delta\mathbf{X}_k = \begin{cases} 0, & k \leqslant n \\ (\mathbf{I} - \mathbf{K}_k\mathbf{H})(\mathbf{\Phi}_{k-1}\Delta\mathbf{X}_{k-1} + \mathbf{\Gamma}G), & k > n \end{cases}. \tag{18}$$

Let $\Delta\mathbf{X}_k = \mathbf{M}_k\mathbf{\Gamma}G$ [17], then

$$M_k = \begin{cases} 0, & k \leqslant n \\ (\mathbf{I} - \mathbb{K}_k\mathbf{H})(\mathbf{\Phi}_{k-1}M_{k-1} + \mathbf{I}), & k > n \end{cases} \tag{19}$$

and

$$\hat{\mathbf{X}}_{k/k} = \begin{cases} \bar{\mathbf{X}}_{k/k}, & k \leqslant n \\ \bar{\mathbf{X}}_{k/k} + M_k\mathbf{\Gamma}G, & k > n \end{cases} \tag{20}$$

where $\mathbf{M}_k$ is recursively computed from equation (19).

Because we are interested in estimating the input of the heat flux magnitude, the analysis require the introduction of the "residual" or "innovation" sequence. The observed value of the residual sequence $\bar{\mathbf{Z}}_k$ with unknown heat flux G can be related to the innovation residual sequence $\hat{\mathbf{Z}}_k$ in the following manner (i.e. if G were known).

$$\bar{\mathbf{Z}}_k = \mathbf{Z}_k - \mathbf{H}\bar{\mathbf{X}}_{k/k-1} = \mathbf{Z}_k - \mathbf{H}\mathbf{\Phi}\bar{\mathbf{X}}_{k-1/k-1} \tag{21}$$

and

$$\hat{\mathbf{Z}}_k = \mathbf{Z}_k - \mathbf{H}\hat{\mathbf{X}}_{k/k-1} = \mathbf{Z}_k - \mathbf{H}\mathbf{\Phi}\hat{\mathbf{X}}_{k-1/k-1} - \mathbf{H}\mathbf{\Gamma}G_{k-1} \tag{22}$$

By subtracting equation (22) from equation (21) and using equation (20), yields

$$\bar{\mathbf{Z}}_k = \begin{cases} \hat{\mathbf{Z}}_k, & k \leqslant n \\ \hat{\mathbf{Z}}_k + \mathbf{B}_k G, & k > n \end{cases} \tag{23}$$

where

$$\mathbf{B}_k = \mathbf{H}(\mathbf{\Phi}M_{k-1} + \mathbf{I})\mathbf{\Gamma}$$

then the equation (23) can be written as

$$\mathbf{Y}_N = \mathbf{B}_N G + \varepsilon_N \tag{24}$$

with

$$\mathbf{Y}_N = [\bar{Z}_{n+1} \quad \bar{Z}_{n+2} \quad , \ldots , \quad \bar{Z}_{n+l}]^{\mathrm{T}}$$

$$\varepsilon_N = [\hat{Z}_{n+1} \quad \hat{Z}_{n+2} \quad , \ldots , \quad \hat{Z}_{n+l}]^{\mathrm{T}}$$

and

$$\mathbf{B}_N = \begin{bmatrix} \mathbf{H}\mathbf{\Gamma} \\ \mathbf{H}(\mathbf{\Phi}\mathbf{M}_{n+1} + \mathbf{I})\mathbf{\Gamma} \\ \vdots \\ \mathbf{H}(\mathbf{\Phi}\mathbf{M}_{n+l-1} + \mathbf{I})\mathbf{\Gamma} \end{bmatrix}.$$

The covariance of the innovation residual sequence $\hat{\mathbf{Z}}$ in the equation (22) is

$$E\{\hat{\mathbf{Z}}_k\hat{\mathbf{Z}}_k^{\mathrm{T}}\} = \mathbf{H}\mathbf{P}_{k/k-1}\mathbf{H}^{\mathrm{T}} + R \triangleq S_k \tag{25}$$

and it is a positive definite matrix.

The covariance of ε_N, by using equation (25), is given by

$$\boldsymbol{\Sigma}_N = \begin{bmatrix} S_{n+1} & 0 & & & \mathbf{O} \\ 0 & S_{n+2} & 0 & & \\ & \cdots & \cdots & & \\ & & \cdots & \cdots & \\ & & 0 & S_{n+l-1} & 0 \\ \mathbf{O} & & & 0 & S_{n+l} \end{bmatrix}. \quad (26)$$

By taking $\boldsymbol{\Sigma}_N^{-1}$ as weighting matrix and according to generalized least squares estimation [20], the estimation heat flux $\hat{G}_N$ can be written as

$$\hat{G}_N = (\mathbf{B}_N^{\mathrm{T}}\boldsymbol{\Sigma}_N^{-1}\mathbf{B}_N)^{-1}\mathbf{B}_N^{\mathrm{T}}\boldsymbol{\Sigma}_N^{-1}\mathbf{Y}_N. \quad (27)$$

Since the elements of ε_N are independent and zero mean random variables with covariance $\boldsymbol{\Sigma}_N$, the least-squares estimation is unbiased. By substituting equation (24) into equation (27), yields

$$E\{\hat{G}_N\} = (\mathbf{B}_N^{\mathrm{T}}\boldsymbol{\Sigma}_N^{-1}\mathbf{B}_N)^{-1}\mathbf{B}_N^{\mathrm{T}}\boldsymbol{\Sigma}_N^{-1}E\{\mathbf{B}_N G+\varepsilon_N\} = G. \quad (28)$$

The covariance of estimation error is

$$P_{bN} = E\{(G-\hat{G}_N)(G-\hat{G}_N)^{\mathrm{T}}\} = (\mathbf{B}_N^{\mathrm{T}}\boldsymbol{\Sigma}_N^{-1}\mathbf{B}_N)^{-1} \quad (29)$$

where

$$G-\hat{G}_N = -(\mathbf{B}_N^{\mathrm{T}}\boldsymbol{\Sigma}_N^{-1}\mathbf{B}_N)^{-1}\mathbf{B}_N^{\mathrm{T}}\boldsymbol{\Sigma}_N^{-1}\varepsilon_N.$$

The weighted least-squares calculation for $\hat{G}_N$, given in equation (27), is referred to as a "batch" calculation. Since the temperature data are acquired sequentially rather than in a batch (i.e. the algorithm must be applied to a situation where the parameters to be estimated are time varying such as a sudden changing in G), equation (27) can be put into a better form for sequential processing of the type described above. One data point is taken for each time step, say N, into equation (27) to calculate G and then the consequences of taking the next observation, say $N+1$, is calculated and so on. The weighting matrix $\boldsymbol{\Sigma}_N^{-1}$ can be modified as

$$\boldsymbol{\Sigma}_N^{-1} = \begin{bmatrix} S_{n+1}^{-1}\gamma^{l-1} & 0 & & & \mathbf{O} \\ 0 & S_{n+2}^{-1}\gamma^{l-2} & 0 & & \\ & \cdots & \cdots & & \\ & & \cdots & \cdots & \\ & & 0 & S_{n+l-1}^{-1}\gamma^{-1} & 0 \\ \mathbf{O} & & & 0 & S_{n+l}^{-1} \end{bmatrix}. \quad (30)$$

To begin, we consider equation (23), the additional of the residual sequence $\bar{Z}_{N+1}$, made at time $k = n+l+1$, becomes available

$$\bar{Z}_{N+1} = \mathbf{B}_{N+1}G+\hat{Z}_{N+1} \quad (31)$$

where $\hat{Z}_{N+1}$ is a new disturbance input and $\mathbf{B}_{N+1}$ can be recursively obtained by equation (23). By combining equation (31) with equation (24), we obtain

$$\mathbf{Y}_{N+1} = \mathbf{B}_{N+1}G+\varepsilon_{N+1} \quad (32)$$

where

$$\mathbf{Y}_{N+1} = \begin{bmatrix} \mathbf{Y}_N \\ \cdots \\ \bar{Z}_{N+1} \end{bmatrix} \quad (33)$$

$$\mathbf{B}_{N+1} = \begin{bmatrix} \mathbf{B}_N \\ \cdots \\ B_{N+1} \end{bmatrix} \quad (34)$$

$$\varepsilon_{N+1} = \begin{bmatrix} \varepsilon_N \\ \cdots \\ \tilde{Z}_{N+1} \end{bmatrix}. \quad (35)$$

The weighting matrix is

$$\boldsymbol{\Sigma}_{N+1}^{-1} = \left[\begin{array}{c:c} \gamma\boldsymbol{\Sigma}_{N+1}^{-1} & 0 \\ \hdashline 0 & S_{N+1}^{-1} \end{array}\right]. \quad (36)$$

By following the same procedure, derived in equation (27), we obtain

$$\hat{G}_{N+1} = (\mathbf{B}_{N+1}^{\mathrm{T}}\boldsymbol{\Sigma}_{N+1}^{-1}\mathbf{B}_{N+1})^{-1}\mathbf{B}_{N+1}^{\mathrm{T}}\boldsymbol{\Sigma}_{N+1}^{-1}\mathbf{Y}_{N+1}. \quad (37)$$

By plugging equations (33)–(34) and equation (36) into equation (37), we yield

$$\hat{G}_{N+1} = (\gamma\mathbf{B}_N^{\mathrm{T}}\boldsymbol{\Sigma}_N^{-1}\mathbf{B}_N+\mathbf{B}_{N+1}^{\mathrm{T}}\mathbf{S}_{N+1}^{-1}\mathbf{B}_{N+1})^{-1} \times (\gamma\mathbf{B}_N^{\mathrm{T}}\boldsymbol{\Sigma}_N^{-1}\mathbf{Y}_N+\mathbf{B}_{N+1}^{\mathrm{T}}\mathbf{S}_{N+1}^{-1}\bar{\mathbf{Z}}_{N+1}). \quad (38)$$

For convenience, we define the matrix $\mathbf{P}_b$

$$\mathbf{P}_{bN+1} = [\mathbf{B}_{N+1}^{\mathrm{T}}\boldsymbol{\Sigma}_{N+1}^{-1}\mathbf{B}_{N+1}]^{-1} = [\gamma\mathbf{G}_N^{-1}+\mathbf{B}_{N+1}^{\mathrm{T}}\mathbf{S}_{N+1}^{-1}\mathbf{B}_{N+1}]^{-1}. \quad (39)$$

Applying the matrix inversion lemma [21], we get the result:

$$\mathbf{P}_{bN+1} = \frac{1}{\gamma}\mathbf{P}_{bN}-\frac{1}{\gamma}\mathbf{P}_{bN}\mathbf{B}_{N+1}^{\mathrm{T}}\left[\frac{\mathbf{B}_{N+1}\mathbf{P}_{bN}\mathbf{B}_{N+1}^{\mathrm{T}}}{\gamma}+\mathbf{S}_{N+1}\right]^{-1}\frac{\mathbf{B}_{N+1}\mathbf{P}_{bN}}{\gamma}. \quad (40)$$

Plugging equation (40) into equation (38) and rearranging it, we obtain

$$\hat{G}_{N+1} = \hat{G}_N+\frac{1}{\gamma}\mathbf{P}_{bN}\mathbf{B}_{N+1}^{\mathrm{T}}\mathbf{S}_{N+1}^{-1}\bar{\mathbf{Z}}_{N+1} -\frac{1}{\gamma}\mathbf{P}_{bN}\mathbf{B}_{N+1}^{\mathrm{T}}\left(\frac{\mathbf{B}_{N+1}\mathbf{P}_{bN}\mathbf{B}_{N+1}^{\mathrm{T}}}{\gamma}+\mathbf{S}_{N+1}\right)^{-1} \times\mathbf{B}_{N+1}\left(\hat{G}_N+\frac{1}{\gamma}\mathbf{P}_{bN}\mathbf{B}_{N+1}^{\mathrm{T}}\mathbf{S}_{N+1}^{-1}\bar{\mathbf{Z}}_{N+1}\right). \quad (41)$$

Then we insert the identity

$$\left(\frac{\mathbf{B}_{N+1}\mathbf{P}_{bN}\mathbf{B}_{N+1}^{\mathrm{T}}}{\gamma}+\mathbf{S}_{N+1}\right)^{-1}\left(\frac{\mathbf{B}_{N+1}\mathbf{P}_{bN}\mathbf{B}_{N+1}^{\mathrm{T}}}{\gamma}+\mathbf{S}_{N+1}\right)$$

between the $\mathbf{B}_{N+1}^{\mathrm{T}}$ and the $\mathbf{S}_{N+1}^{-1}$ in the second term on the right-hand-side of equation (41). Then, we multiply $\bar{\mathbf{Z}}_{N+1}$ to equation (41), and let $N+1$ be replaced by k, we obtain a recursive input estimator $\hat{G}_k$

$$\hat{G}_k = \hat{G}_{k-1}+\mathbf{K}_{bk}(\bar{\mathbf{Z}}_k-\mathbf{B}_k\hat{G}_{k-1}) \tag{42}$$

where

$$\mathbf{K}_{bk}=\frac{\mathbf{P}_{bk-1}\mathbf{B}_k^{\mathrm{T}}}{\gamma}\left(\mathbf{S}_k+\frac{\mathbf{B}_k\mathbf{P}_{bk-1}\mathbf{B}_k^{\mathrm{T}}}{\gamma}\right)^{-1}$$

and

$$\mathbf{P}_{bk}=\frac{1}{\gamma}(\mathbf{I}-\mathbf{K}_{bk}\mathbf{B}_k)\mathbf{P}_{bk-1}.$$

From the above derivation, it simply indicates that the new estimate is expressed by the old estimate plus a correction term. The algorithm effectively improves the computational efficiency drastically for updating the estimate $\hat{G}_k$. A scalar parameter γ, $0<\gamma\leqslant 1$, is used in this algorithm. For $\gamma=1$, it is suitable only for constant parameter system. For the time-varying case, the factor γ can be taken between 0 and 1, therefore, the corresponding algorithm can preserve its updating ability continuously. In the estimation problem, the Kalman filter requires an exact knowledge of the process noise covariance Q and the measurement noise covariance R. Usually, the R depends on the measurements of sensor. Both the value of Q in the filter and the value of γ in sequential least squares approach will interactively affect fast adaptive capability for tracking time-varying parameter. In general, if we select the large value of Q then the γ could be chosen near 1 then the filter memory becomes long, and noise effects are reduced; whereas for smaller γ, the memory is short and the estimation can track the sudden changes that occur in heat flux, G, such as an impulse boundary heat flux simulation.

3. EXPERIMENTAL APPARATUS AND PROCEDURE

A schematic diagram of a computer-based data acquisition system, used for the temperature measurement, is shown in Fig. 2. The changing analog voltage signal is detected by a thermocouple and a differential amplifier with a gain of 500. The signals are taken and recorded with the PCL-1800 data acquisition board. The resolution of the data acquisition hardware is approximately 0.1°C with 125 Hz sample rate.

In order to achieve an adiabatic boundary condition at $X=X_s$, the silastic rubber is impregnated into the space between the ABS tube and insulator (in Fig. 3). The copper plate is 0.5 or 1.0 mm in thickness and 8 mm diameter. A thermocouple of type K is welded to the rear surface with M42 primer ignited at the opposite side. This is carried out for M42 primer at a range of distances (standoff distance) 0, 13, 26 and 30 mm, respectively.

4. RESULTS AND DISCUSSIONS

Before we implement the RLSA with experimental data to estimate the heat flux, generated from the M42 primer, we first use RLSA method in the following simulation for an impulse boundary heat flux to test its adequacy. The physical model is the same as equations

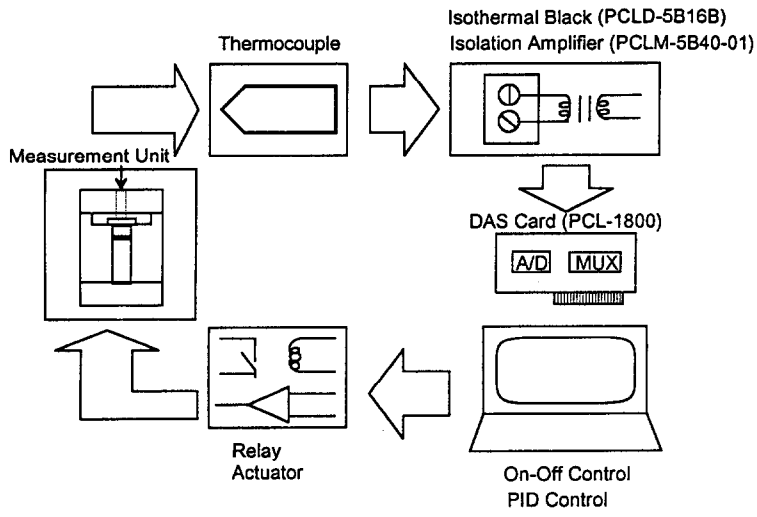

Fig. 2. Schematic diagram of the experimental facility.

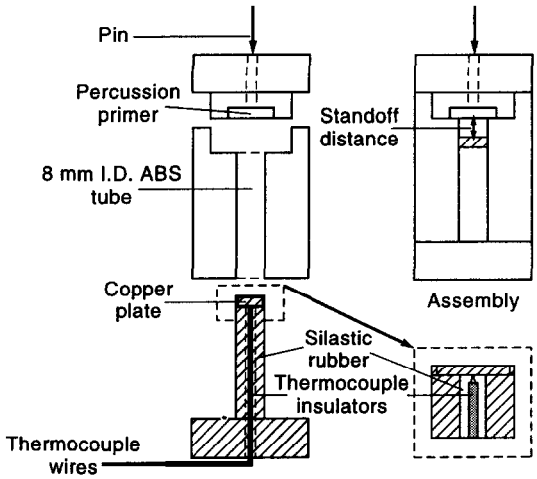

Fig. 3. Measurement unit.

(1)–(5) and assumes that exact boundary heat flux $G(t)$ to be estimated is described as follows

$$G(t) = \begin{cases} 0, \\ \quad 0 \leqslant t < 0.32 \text{ or } 0.44 \leqslant t \leqslant t_f \\ 10 * (t - 0.32)/0.04, \\ \quad 0.32 \leqslant t < 0.36 \\ 10 * (1 - (t - 0.36)/0.08), \\ \quad 0.36 \leqslant t < 0.44 \end{cases} \quad (43)$$

The simulation conditions and the parameters are given by the following: sampling interval $\Delta t = 0.008$ [s]; copper plate thickness = 0.05 [cm]; space increment $\Delta X = 0.005$ [cm]; thermal diffusivity $\alpha = 0.1804$ [cm^2 s^{-1}]; thermal conductivity $\kappa = 0.145696$ [cal cm^{-1} s^{-1}°C]; process noise covariance $Q = 0.025$; measurement noise covariance $R = 0.0625$; fading factor $\gamma = 0.01$.

The results of inverse solution, obtained by the RLSA are shown in Fig. 4. The estimation is in excellent agreement with the exact results. The root mean square errors (RMS) between the exact heat flux and the estimated heat flux is 0.2421 [cal cm^{-2}–s^{-1}]. All the calculations in this work are performed on a personal computer (PC-486).

To illustrate the application and the accuracy of the RLSA method, we consider eight specific experiments involving the estimation of the timewise variation of the strength of a surface heat flux, located at the foreside of a copper plate and the transient temperature recording taken at the opposite boundary surface. Initially, the copper plate is at ambient temperature, T_0, the rear surface boundary is kept insulated, and the M42 primer acting at foreside side (see Fig. 3).

For copper plate thickness = 0.5 mm, the standoff distance is taken as 0 mm first. The experimental measured temperature/time profile for M42 primer is shown in Fig. 5(a). These data are analyzed on-line to estimate the corresponding heat flux which is calculated by the RLSA, as described above. The physical parameters in this study are taken as space increment $dx = 0.05$ mm, time increment $dt = 0.008$ s, thermal

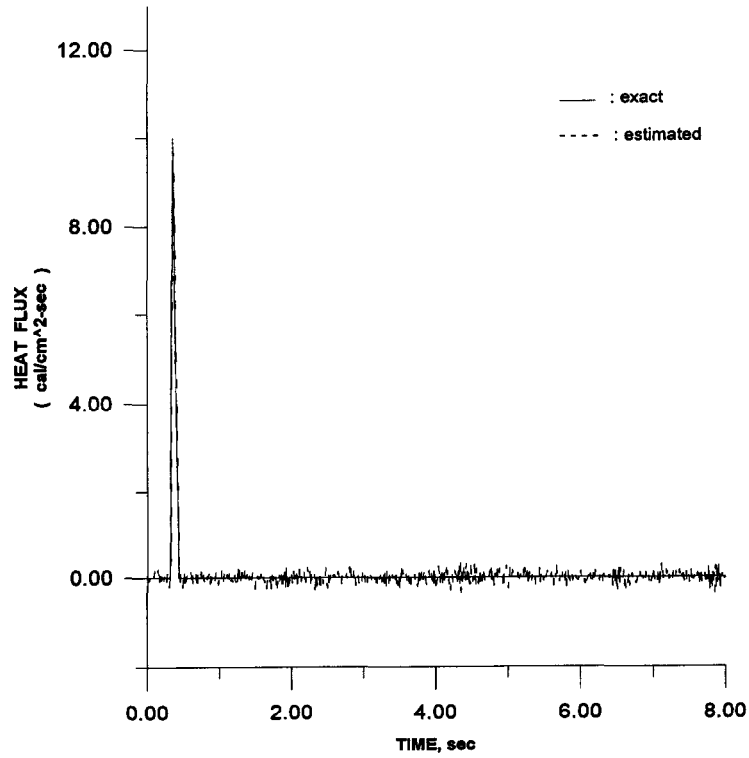

Fig. 4. ELSA estimated of the timewise variation of the strength of a boundary heat flux, for the filter model order $N = 11$ with measurement noise covariance level, $R\ (=\sigma^2) = 0.0625$.

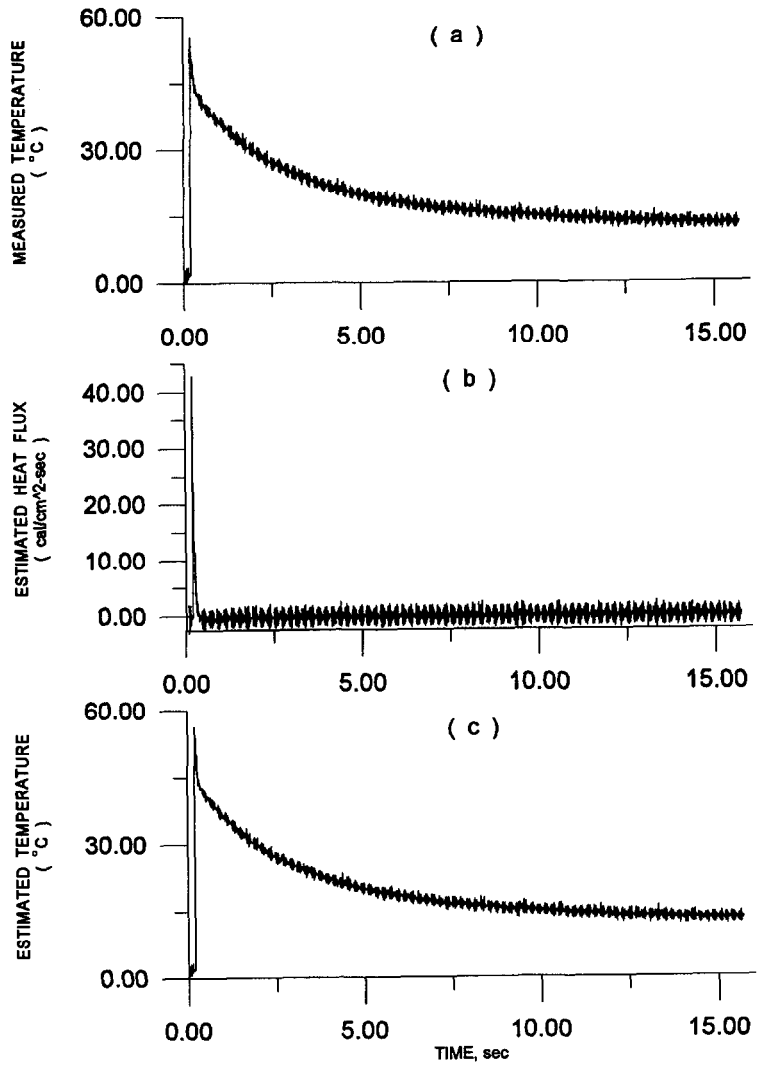

Fig. 5. Copper plate thickness = 0.5 mm, standoff distance = 0 mm: (a) experimental measured temperature for M42 primer; (b) estimated surface heat flux by RLSA; (c) temperature profiles at $x = x_s$ by DHCP with estimated surface heat flux in (b), as input.

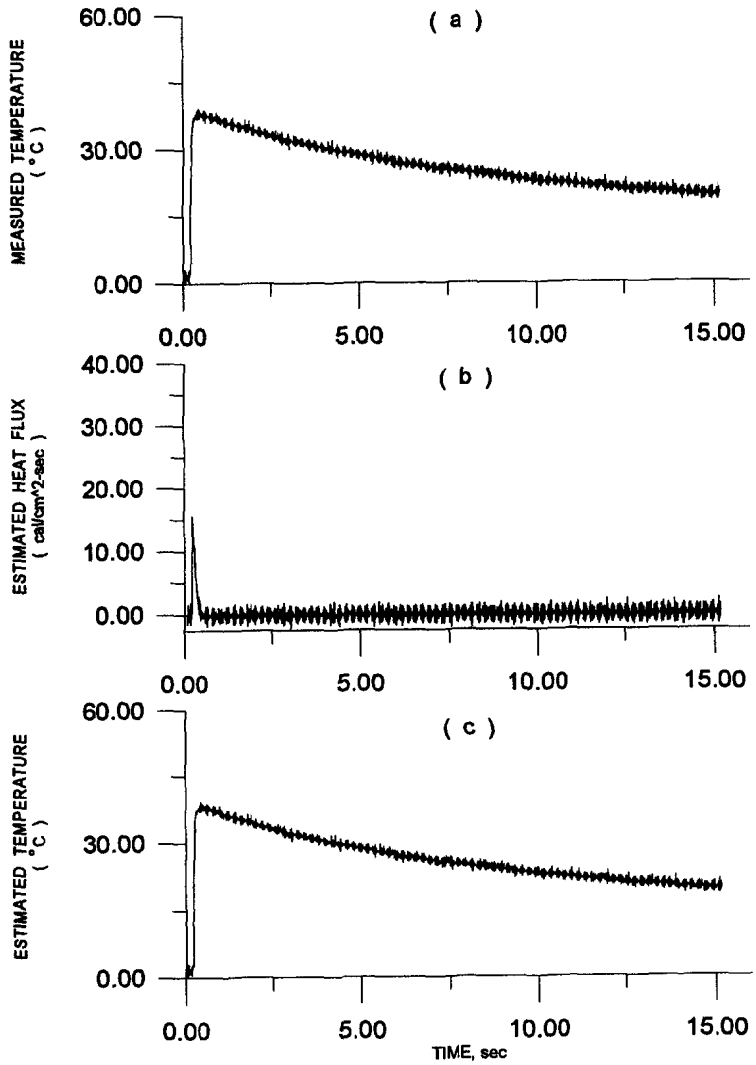

Fig. 6. Copper plate thickness = 0.5 mm, standoff distance = 13 mm: (a) experimental measured temperature for M42 primer; (b) estimated surface heat flux by RLSA; (c) temperature profiles at $x = x_s$ by DHCP with estimated surface heat flux in (b), as input.

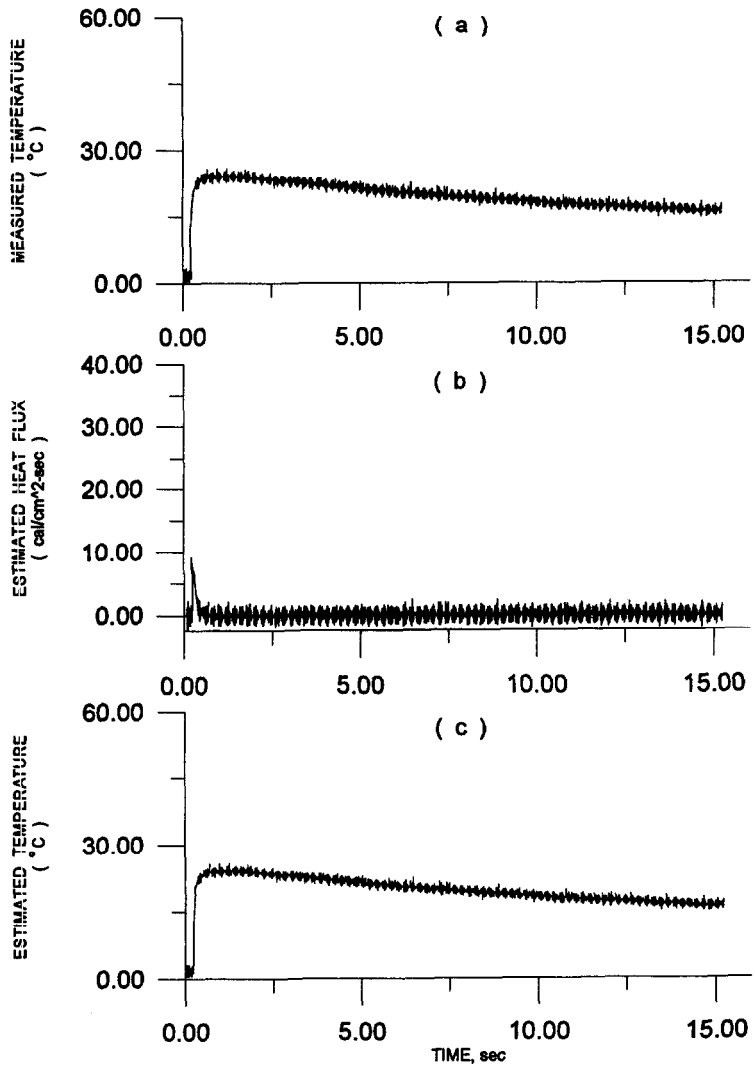

Fig. 7. Copper plate thickness = 0.5 mm, standoff distance = 26 mm: (a) experimental measured temperature for M42 primer; (b) estimated surface heat flux by RLSA; (c) temperature profiles at $x = x_s$ by DHCP with estimated surface heat flux in (b), as input.

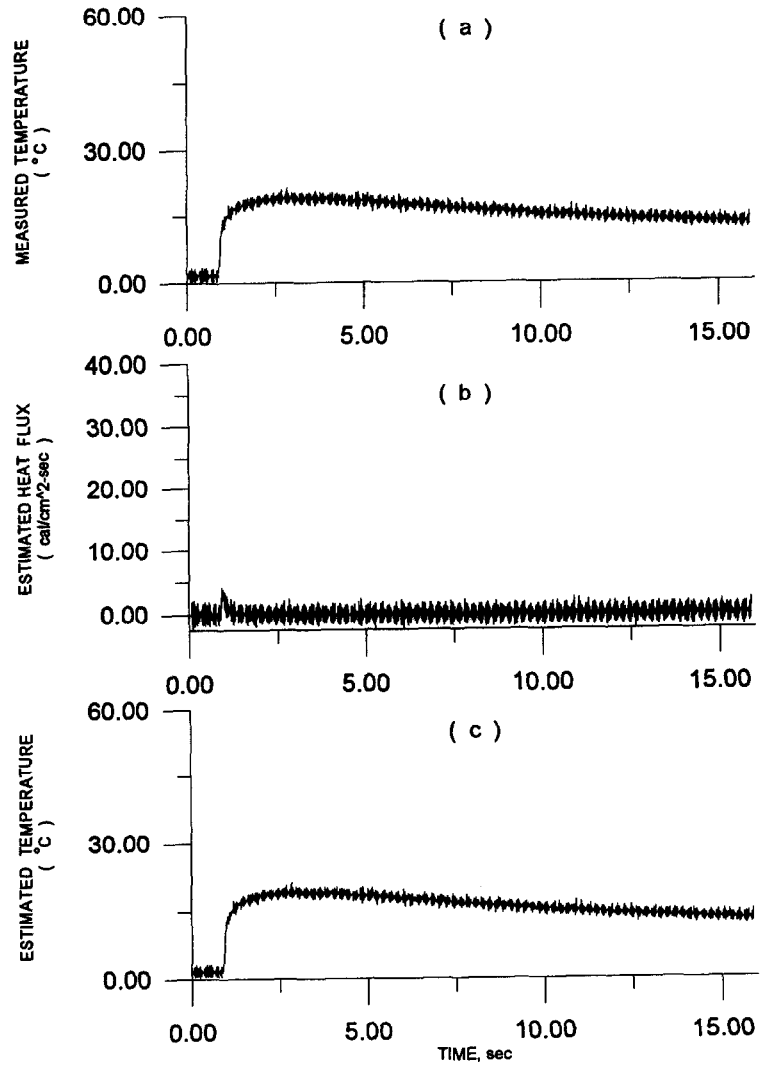

Fig. 8. Copper plate thickness = 0.5 mm, standoff distance = 30 mm: (a) experimental measured temperature for M42 primer; (b) estimated surface heat flux by RLSA; (c) temperature profiles at $x = x_s$ by DHCP with estimated surface heat flux in (b), as input.

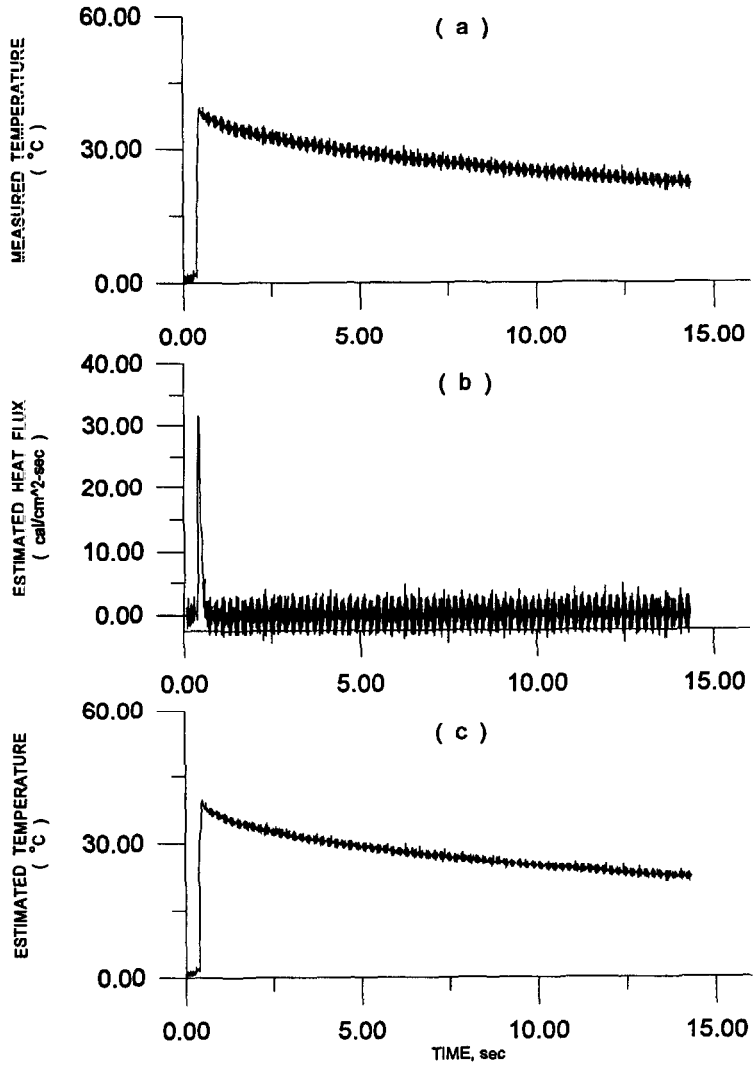

Fig. 9. Copper plate thickness = 1.0 mm, standoff distance = 0 mm: (a) experimental measured temperature for M42 primer; (b) estimated surface heat flux by RLSA; (c) temperature profiles at $x = x_s$ by DHCP with estimated surface heat flux in (b), as input.

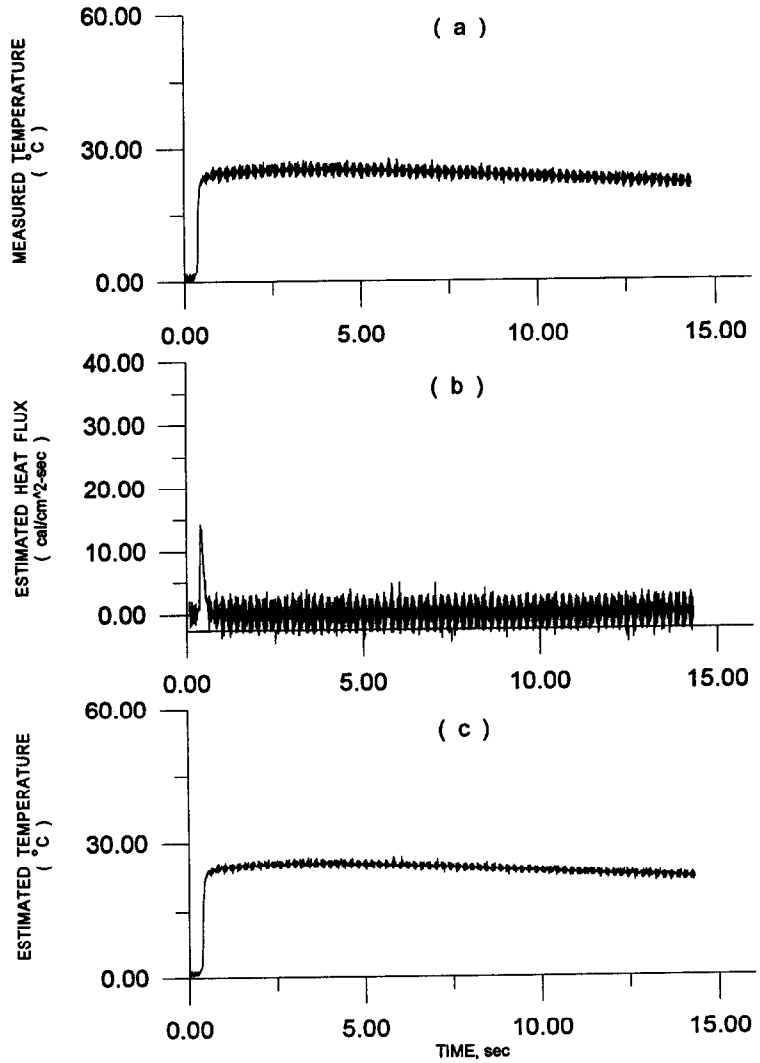

Fig. 10. Copper plate thickness = 1.0 mm, standoff distance = 13 mm: (a) experimental measured temperature for M42 primer; (b) estimated surface heat flux by RLSA; (c) temperature profiles at $x = x_s$ by DHCP with estimated surface heat flux in (b), as input.

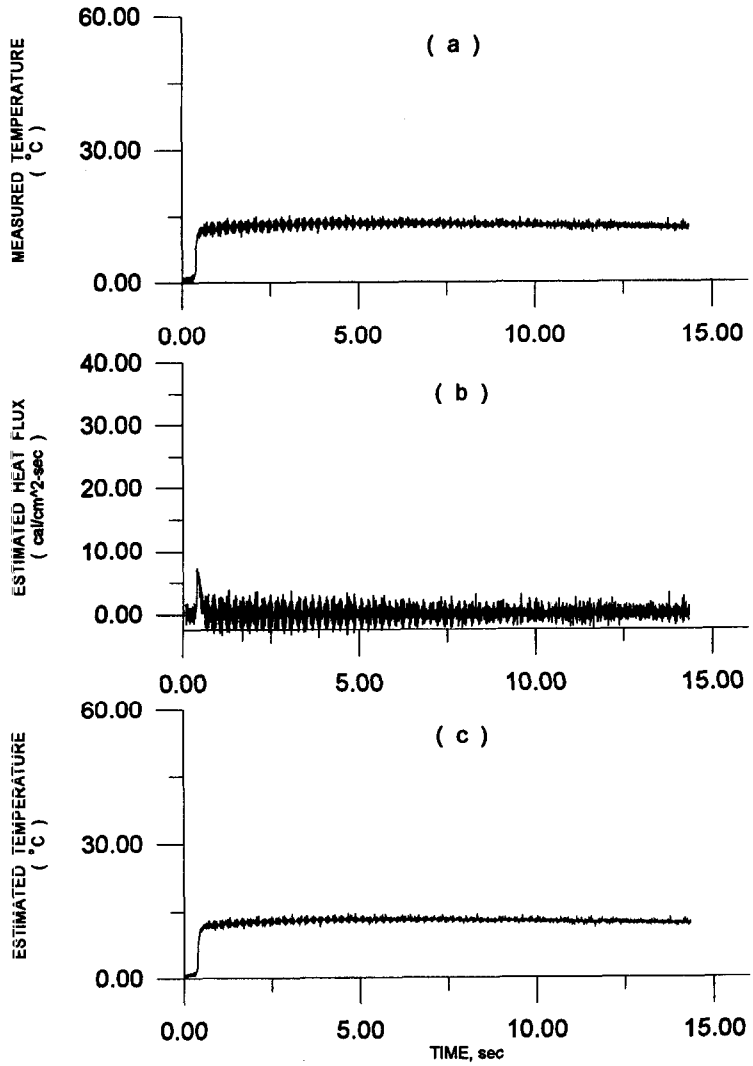

Fig. 11. Copper plate thickness = 1.0 mm, standoff distance = 26 mm: (a) experimental measured temperature for M42 primer; (b) estimated surface heat flux by RLSA; (c) temperature profiles at $x = x_s$ by DHCP with estimated surface heat flux in (b), as input.

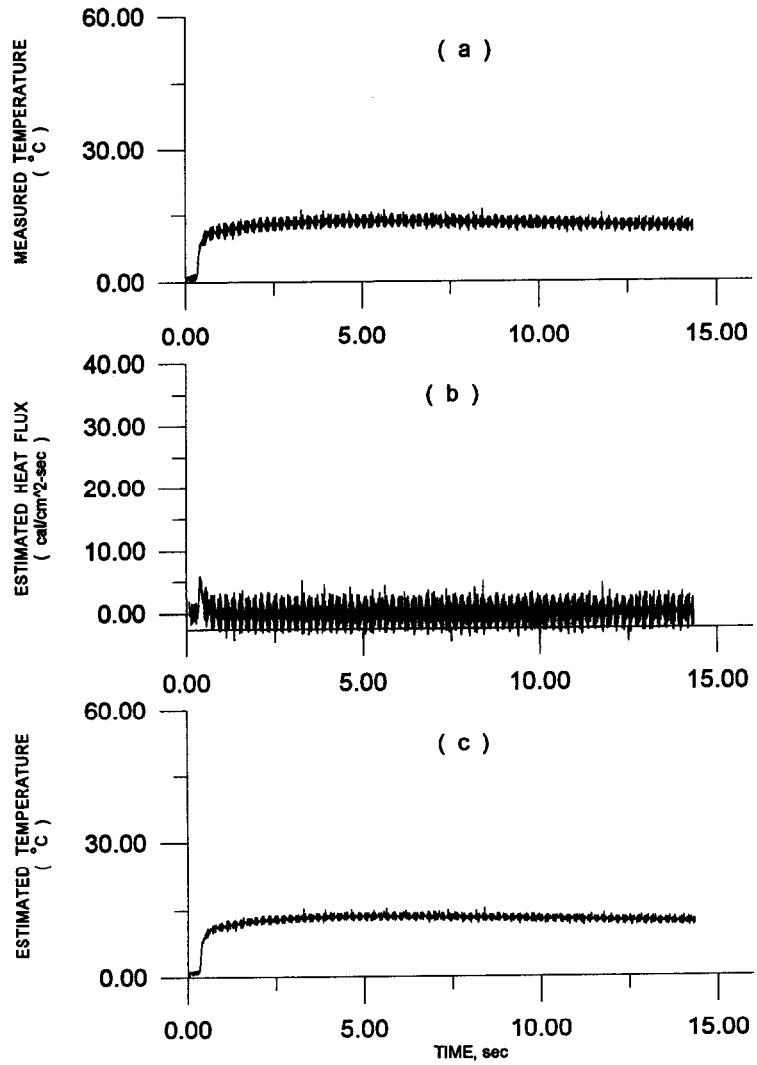

Fig. 12. Copper plate thickness = 1.0 mm, standoff distance = 30 mm: (a) experimental measured temperature for M42 primer; (b) estimated surface heat flux by RLSA; (c) temperature profiles at $x = x_s$ by DHCP with estimated surface heat flux in (b), as input.

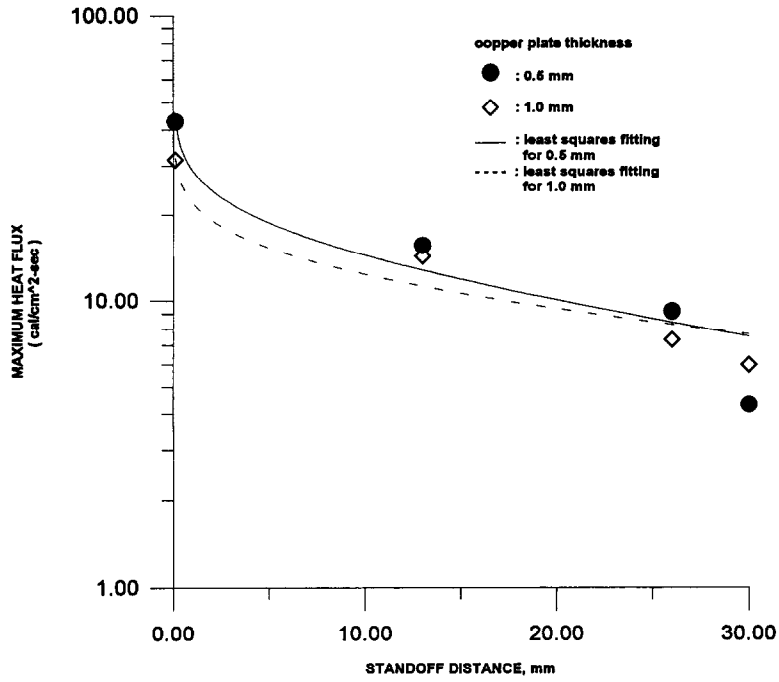

Fig. 13. Maximum heat flux and least squares fitting vs standoff distance for the different thickness.

diffusivity $\alpha = 0.1804$ [cm^2 s^{-1}], and the thermal conductivity $\kappa = 0.145696$ [cal cm^{-1}]. The initial conditions for the recursive input estimator are given by

$$\hat{\mathbf{X}}_{-1/-1} = [0 \quad 0 \quad ,\ldots, \quad 0]^{\mathrm{T}}, \quad \mathbf{P}_{-1/-1} = \mathrm{diag}\,[10^{10}],$$

$$\hat{G}_{-1} = 0, \quad \mathbf{P}b_{-1} = 10^{8}$$

and $\mathbf{M}_{-1}$ is set by zero matrix.

The process noise covariance, the measurement noise and the fading factor are taken to $Q = 50$, $R = 0.0625$ and $\gamma = 0.87$, respectively, in all cases. The resulting of IHCP, obtained by the RLSA, with measured temperature in Fig. 5(a), is shown in Fig. 5(b). In order to facilitate the comparison and to judge the estimated heat flux, the value of estimated heat flux, in Fig. 5(b), is used as input, at $x = 0$ and DHCP is used to solve estimated temperature history, at $x = x_s$ which is plotted in Fig. 5(c). The history of the estimated temperature history calculated by using DHCP, Fig. 5(c), is the same as that of the corresponding measured temperature in Fig. 5(a). Therefore, it shows that the estimated heat flux is the heat flux generated by the M42 primer on the foreside copper plate surface. The RMS value is 0.15 (°C) calculated from measured temperature and estimated temperature.

The effects of the alternating magnitude of heat flux on the accuracy of estimations were also tested by changing the standoff distance from 0 to 13 mm, 26 mm and 30 mm, respectively. These three temperature histories, in Figs. 6–8(a), show a decrease in measured temperature with the increasing standoff distance as expected. The results, estimated surface heat flux, are presented in Figs. 6–8(b). It is shown that the maximum estimated heat flux decreases as the standoff distance increases. The RMS values between the measured temperature, in Figs. 6–8(a), and the estimated temperature, in Figs. 6–8(c), are 0.11, 0.12, 0.13 and 0.10 (°C), respectively.

The second example is the same as that considered in example 1, except the copper plate thickness is taken as 1.0 mm instead of 0.5 mm. The physical properties and system model parameters are kept unchanged. The measured temperature, estimated heat flux, and estimated temperature are presented in Figs. 9–12. The RMS values are 0.43, 0.41, 0.29 and 0.41 (°C) with standoff distance = 0.0, 13, 26 and 30 mm, respectively.

In Fig. 13, we show the maximum estimated heat flux verse standoff distance for different thicknesses, 0.5 and 1.0 mm. With all these data, the least squares fit of the equations for the different thicknesses, 0.5 and 1.0 mm, are $\log(G) = -6.26764\log(X) + 28.8506$ (solid line) with 9.71963 residual mean square and 19.4393 residual sum of squares, $\log(G) = -4.25397\log(X) + 22.1436$ (dotted line) with

6.76695 residual mean square and 13.5339 residual sum of squares, respectively.

5. CONCLUSIONS

The conclusions derived from this work can be summarized as follows:

(1) A sharp impulse form of input can be estimated very precisely by means of the RLSA.

(2) The RLSA is adequate for on-line 1-D inverse heat conduction experimental estimation.

(3) The relation between the physical model and the process noise covariance (Q) needs further study.

REFERENCES

1. Stolz, G., Numerical solutions to an inverse problem of heat conduction for simple shapes. *Transactions of ASME, Journal of Heat Transfer*, 1960, **82C**, 20–26.
2. Sparrow, E. M., Haji-Sheikh, A. and Lundgren, T. S., The inverse problem in transient heat conduction. *Transactions of ASME, Journal of Applied Mechanics*, 1964, **86E**, 369–375.
3. Beck, J. V., Surface heat flux determination using an integral method. *Nuclear Engineering Design*, 1968, **7**, 170–178.
4. Imber, M. and Khan, J., Prediction of transient temperature distributions with embedded thermocouples. *AIAA Journal*, 1972, **10**, 784–789.
5. Woo, K. C. and Chow, L. C., Inverse heat conduction by direct inverse laplace transform. *Numerical Heat Transfer*, 1981, **4**, 499–504.
6. Beck, J. V., Blackwell, B. and St. Clair, C. R., *Inverse Heat Conduction*. Wiley, New York, 1985.
7. Beck, J. V., Determination of undisturbed temperatures from thermocouple measurements using correction kernels. *Nuclear Engineering Design*, 1968, **7**, 9–12.
8. Beck, J. V., Nonlinear estimation applied to the nonlinear inverse heat conduction problem. *International Journal of Heat and Mass Transfer*, 1970, **13**, 703–716.
9. Blackwell, B. F., Efficient technique for the numerical solution of one-dimensional inverse problem of heat conduction. *Numerical Heat Transfer*, 1981, **4**, 229–238.
10. Alifanov, O. M. and Mikhailov, V. V., Solution of the nonlinear inverse thermal conductivity problem by the iteration method. *Journal of Engineering Physics*, 1978, **35**, 1501–1506.
11. Jarny, Y., Özisik, M. N. and Bardon, J. P., A general optimization method using adjoint equation for solving multidimensional inverse heat conduction. *International Journal of Heat and Mass Transfer*, 1991, **34**, 2911–2919.
12. Huang, C. H. and Özisik, M. N., Inverse problem of determining the unknown strength of an internal plane heat source. *Journal of the Franklin Institute*, 1992, **329**(4), 751–764.
13. Silva Neto, A. J. and Özisik, M. V., Simultaneous estimation of location and timewise-varying strength of a plane heat source. *Numerical Heat Transfer, Part A*, 1993, **24**, 467–477.
14. Bokar, J. C., Özisik, M. N., An inverse analysis for estimating the time-varying inlet temperature in laminar flow inside a parallel plate duct. *International Journal of Heat and Mass Transfer*, 1995, **38**(1), 39–45.
15. Chan, Y. T., Hu, A. G. C. and Plant, J. B., A Kalman filter based tracking scheme with input estimation. *IEEE Transactions on Aerospace and Electronic Systems*, 1979, **AES-15**, 237–244.
16. Hou, M. and Xian, S., Comments on tracking a maneuvering target using input estimation. *IEEE Transactions on Aerospace and Electronic Systems*, 1989, **AES-25**(2), 280.
17. Bogler, P. L., Tracking a maneuvering target using input estimation. *IEEE Transactions on Aerospace and Electronic Systems*, 1987, **AES-23**(3), 298–310.
18. Farooo, M. and Bruder, S., Comments on tracking a maneuvering target using input estimation. *IEEE Transactions on Aerospace and Electronic Systems*, 1989, **AES-25**(2), 300–302.
19. Tuan, P. C., Ji, C. C., Fong, L. W. and Huang, W. T., An input estimation approach to on-line two-dimensional inverse heat conduction problem. *Numerical Heat Transfer B*, 1996 (submitted).
20. Franklin, G. F., Powell, J. D. and Workman, M. L., *Digital control of Dynamic Systems*, 2nd edn. Addison-Wesley, Reading, MA, 1990.
21. Mendel, J. M., *Lessons in Digital Estimation Theory*. Prentice-Hall, Englewood Cliffs, N.J., 1987.